Tunable thermal transport and thermal rectification in strained graphene nanoribbons

K. G. S. H. Gunawardana,[1,*] Kieran Mullen,[1] Jiuning Hu,[2] Yong P. Chen,[2,3] and Xiulin Ruan[4]

[1]*Homer L. Dodge Department of Physics and Astronomy, Center for Semiconductor Physics in Nanostructures, The University of Oklahoma, Norman, Oklahoma 73069, USA*

[2]*Birk Nanotechnology Center and School of Electrical and Computer Engineering, Purdue University, West Lafayette, Indiana 47907, USA*

[3]*Birk Nanotechnology Center and Department of Physics, Purdue University, West Lafayette, Indiana 47907, USA*

[4]*Birk Nanotechnology Center and School of Mechanical Engineering, Purdue University, West Lafayette, Indiana 47907, USA*

Using molecular dynamics (MD) simulations, we study thermal transport in graphene nanoribbons (GNR) subjected to uniform uniaxial and nonuniform strain fields. We predict significant thermal rectification (over 70%) in a rectangular armchair GNR by applying a transverse force asymmetrically. The heat flux is larger from the less stressed region to the more stressed region. Furthermore, we develop a theoretical framework based on the nonequilibrium thermodynamics to discuss when thermal rectification under a stress gradient can occur. We conclude with a discussion of details relevant to experiment.

PACS number(s): 65.80.Ck, 44.10.+i, 44.35.+c

I. INTRODUCTION

Operation of nanoscale thermal devices, mainly relies on the tunability of phonon transport by external means. Thermal devices such as thermal rectifiers,[1] thermal transistors,[2] and thermal memories[3] are a new class of devices, whose operation is driven by the temperature gradients. These devices will have useful applications not only in thermal circuits[4] but also in nanoscale thermal management and thermoelectric applications.

A thermal rectifier, in which the thermal current is larger in one direction than in the opposite, is one of the most fundamental thermal devices to be realized experimentally in nanoscale. Thermal rectification has been demonstrated using molecular dynamics simulations (MD) in asymmetric systems and is discussed as resulting from an interplay between structural asymmetry and lattice anharmonicity.[1,5,6] Recently, this phenomenon has been observed experimentally in asymmetrically mass-loaded carbon and boron nitride nanotubes.[7] Moreover, thermal rectification has been predicted in triangular and trapezoidal shaped graphene nanoribbons (GNRs).[5,6] In this paper, we introduce a method based on strain engineering as an experimentally feasible approach to realize significant (>70%) thermal rectification in GNRs. The potentially real-time tunability of the thermal rectification is a distinctive advantage of this approach.

Graphene is a promising material for nanoscale applications due to its exceptional electronic,[8] thermal,[9] and mechanical[10] properties. It has been shown recently that the electronic properties of graphene can be tuned significantly by engineering strain. For instance, strain could produce a pseudomagnetic field[11–13] that affects the electronic properties of graphene. Furthermore, strain could induce semiconducting properties on metallic GNRs by opening a gap in the electronic band structure.[14] However, strain-induced tuning of thermal transport properties of graphene has been less studied. The effect of uniform uniaxial strains on the thermal conductivity (κ) of graphene has been studied recently by MD simulations and the reported effect is substantial in tuning κ.[15]

When increasing the uniaxial tensile strain [arrows in Fig. 1(a)], we observe broadening the gap in the phonon dispersion of armchair GNR (AGNR) whereas the effect on the phonon dispersion of zigzag GNR (ZGNR) is mild. The calculated κ of AGNR also reduce considerably when increasing the tensile strain compared to that of ZGNR. We predict thermal rectification on an asymmetrically stressed rectangular GNR. In our system, asymmetric stress is achieved by exerting a transverse force (F_y) on the top and bottom edge atoms of part (for example, the right half) of the AGNR as illustrated in Fig. 1(b). We observe that the thermal current is larger from the less stressed to the more stressed region (left to right) than that in the opposite direction (right to left). Furthermore, we develop a theoretical framework based on the nonequilibrium thermodynamics to model thermal rectification in the presence of a stress gradient.

II. SIMULATION PROCEDURE

Figure 1 shows a schematic of n-ZGNR (Zigzag GNR) and n-AGNR structures simulated. The carbon-carbon bond length is 1.42 Å in the absence of strains. The n refer to the number of carbon dimers (a dimer is shown by the oval) in width.[16] The first and the last columns of atoms are fixed and the adjacent three columns of atoms of the n-ZGNR and four columns of atoms of the n-AGNR are coupled to the Nosé-Hoover thermostats. In the MD simulation, a second-generation Brenner potential[17] is employed to describe the carbon-carbon interactions. The equations of motion are integrated using the third-order predictor-corrector method. The time step is 0.5 fs and the total simulation time is 5 ns (10^7 time steps). The temperatures of the left and right heat baths (HBs) are set to T_L and T_R respectively. The temperature difference $(T_L - T_R) = 2\alpha T$, where α determines the temperature bias and the average temperature $T = (T_L + T_R)/2$. The net heat flux (J) was calculated by the power delivered by the heat baths.[18] The thermal conductivity (κ) of the system is calculated according to Fourier's law, $J = \kappa wh\nabla T$, where w and h are width and van der Waals thickness ($h = 0.335$ nm) of the GNR.

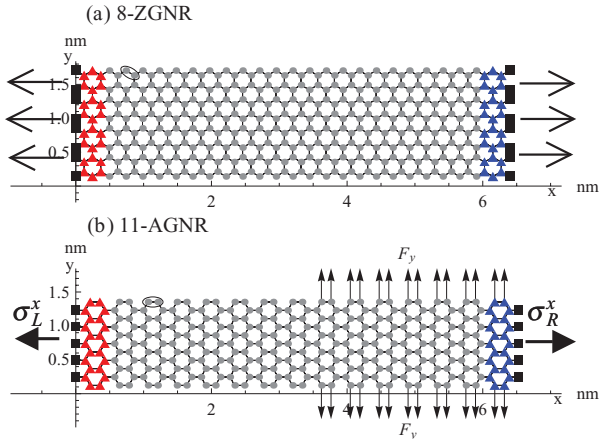## (a) 8-ZGNR

(b) 11-AGNR

FIG. 1. (Color online) Schematic of the 8-ZGNR (a) and 11-AGNR (b). The triangles represent the thermostated atoms and the full squares are the fixed atoms. The horizontal arrows in (a) shows the direction of uniaxial tensile strain. In (b), the vertical arrows show the applied constant force F_y on the top and bottom atoms of the right half of the AGNR. The horizontal arrows in (b) represent the stress developed in length (x) direction (σ_R^x and σ_L^x) near the heat baths.

III. THERMAL TRANSPORT UNDER UNIFORM STRAIN FIELDS

Figure 2 shows the variation of κ/κ_0 of ZGNRs and AGNRs of two different widths as a function of strain ranging from -0.03 to 0.12. The κ_0 is the thermal conductivity of unstrained nanoribbon. The horizontal arrows in Fig. 1(a) show the direction of uniaxial tensile strain on both nanoribbons. The strain is given by $(l - l_0)/l_0$, where l is the stretched or compressed length and l_0 is the initial length of the sample. Strain is applied by slowly moving the fixed atoms on one side (right side) at a rate of $\pm 1.0 \times 10^{-6}$ Å per time step at 300 K. The calculated values of the thermal conductivity (κ_0) of unstrained 8-ZGNR, 12-ZGNR, 11-AGNR, and 19-AGNR are 5360, 5500, 3300, and 3600 W/mK, respectively. The variation of κ for ZGNRs in the range of strain 0–0.1 is about 30% from the unstrained values. The reduction of κ at a strain of 0.1 is about 55% for 11-AGNR and 19-AGNR. Figure 3 shows the calculated phonon dispersions of 8-ZGNR and 11-AGNR along the transport direction (x) of unstrained nanoribbons and at a strain of 0.024. When increasing the uniaxial tensile strain, we do not observe a significant alteration
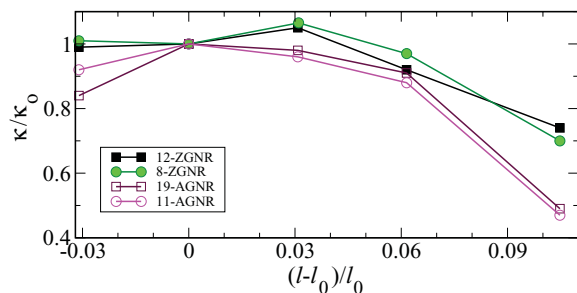

FIG. 2. (Color online) Normalized thermal conductivity (κ/κ_0) as a function of uniaxial strain ($l - l_0)/l_0$ along the transport direction (x) calculated at 300 K.
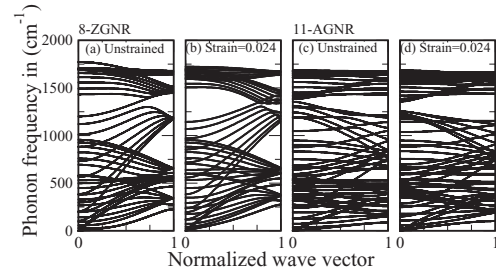

FIG. 3. Phonon dispersion of 8-ZGNR and 11-AGNR under uniaxial tensile strains. The horizontal axis is the normalized wave vector projected on to the transport direction (x).

of dispersion curves of the 8-ZGNR [see Figs. 3(a) and 3(b)]. However, we observe an increased of the phonon velocity ($d\omega/dk$) of some modes in the low (0–600 cm^{-1}) and high (1250–1600 cm^{-1}) frequencies, which could be the reason for the increment of the κ in small strains. In 11-AGNR, we observe broadening the narrow gap at 1350 cm^{-1} in the phonon dispersion. At a strain of 0.024, we observe a gap in the frequency range 1250–1350 cm^{-1} [see Fig. 3(d)]. The gap further broadens and moves toward low frequencies when increasing the uniaxial strain. This could be the reasons for the relatively larger reduction of κ of AGNR with increasing strain.

IV. THERMAL TRANSPORT UNDER NONUNIFORM STRAIN FIELDS

In many of the theoretical studies on thermal transport, the stress along the nanoribbon is considered to be uniform and uniaxial. We consider a situation that the stress at the left and right edges of the nanoribbon are σ_L and σ_R such that $\sigma_L \neq \sigma_R$. In the intermediate region, it is assumed to vary smoothly. This kind of stress profile could possibly be realized experimentally using the differential thermal expansion of graphene grown on structured substrates[13,19,20] or through externally applied strain.[21] We achieve such an asymmetric stress profile in our simulation by transversely stressing a half of the GNR. For example, we apply a constant force F_y on the atoms of the top and bottom edges of the right half of the 11- AGNR as depicted in Fig. 1(b). The tensile stress developed across the y direction of the right half is denoted by σ_R^y. This lateral stress produces a tensile strain along the y direction and, hence a compressive strain along the x direction due to the Poisson contraction. Since the atoms in the left and right edges are fixed, this compressive strain also results in tensile stress in the x direction. The stress in the x direction near the left and right HB is denoted by σ_L^x and σ_R^x. This is calculated from the time average of the forces on the fixed atoms at the left and right edges (excluding the corner atoms). Figure 4(a) shows the variation of σ_L^x and σ_R^x on F_y calculated at $T = 300$ K. The σ_L^x and σ_R^x are tensile, and σ_L^x is smaller than the σ_R^x, while both are found to be increasing with F_y.

A. Thermal rectification

In Fig. 5(a), the thermal current from left to right ($+\alpha$) and right to left ($-\alpha$) are plotted against the applied force F_y, when $|\alpha| = 0.3$ and $T = 300$ K. The thermal current from left to
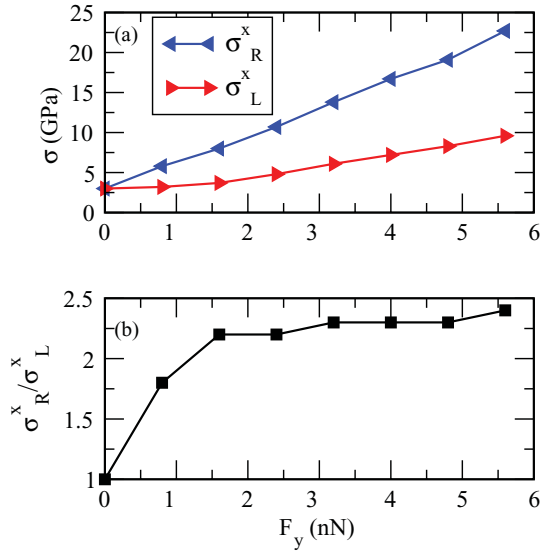
FIG. 4. (Color online) (a) Variation of stresses (σ_R^x and σ_L^x) on the 11-AGNR as a function of F_y. These are the stresses in the center part of the nanoribbon near the right and left heat baths. (b) The ratio σ_R^x/σ_L^x as a function of F_y. The units of F_y are in nano-Newtons (nN).

right ($J_{L\to R}$) shows very small decrement, whereas the $J_{R\to L}$ decreases significantly when F_y is increased. Thus the $J_{L\to R}$ is considerably larger than $J_{R\to L}$ whenever $F_y > 0$, marking the existence of thermal rectification in this system.

The tensile stress and strain can affect the thermal transport by distorting the lattice to both alter the characteristic vibrational frequencies and the degree of anharmonicity.[22] Anharmonicity is essential: *no amount of geometric or parameter asymmetry can produce thermal rectification.* Without anharmonicity, the system can be analyzed via normal modes, and time reversal symmetry will require that transmission amplitudes from left to right are the same as right to left. We attribute the observed thermal rectification to the strain
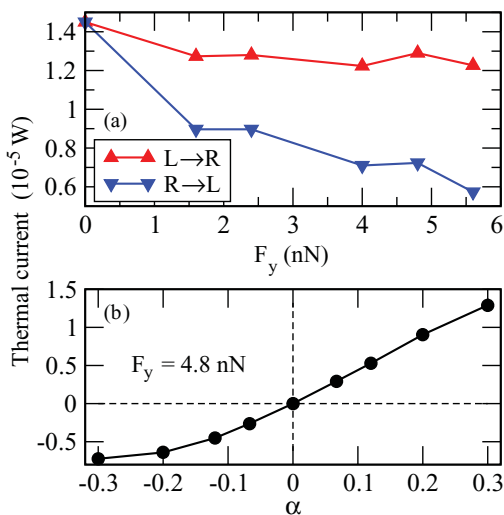

FIG. 5. (Color online) (a) Thermal current from left to right and right to left as a function of F_y at $T = 300$ K and $|\alpha| = 0.3$, and (b) Variation of thermal current with the temperature bias (α) at $F_y = 4.8$ nN.

induced asymmetry of the vibrational frequencies and the lattice anharmonicity. Such an asymmetry of the vibrational properties leads to a local variation of κ. It can be shown that the thermal conductivity must be a function of both position and temperature to rectify the thermal current.[23]

We can invoke the framework of nonequilibrium thermodynamics to describe this effect. The change of the entropy per unit volume of a solid due to the applied stress (τ_α) can be expressed,[24] $ds = \frac{du}{T} - \frac{1}{T}\sum_\alpha \tau_\alpha d\eta_\alpha$, where du is the change of internal energy density, η_α is the strain and $\alpha \in [xx, yy, xy]$. From this, we can deduce the rate of production of entropy,[25]

$$\dot{s} = \partial_i \left(\frac{1}{T}\right) J_i^{(u)} + \frac{1}{T}\partial_i (\tau_\alpha) J_i^{(\eta_\alpha)}, \quad (1)$$

where $J_i^{(u)}$ and $J^{(\eta_\alpha)}$ are the ith components of the energy and the strain currents, and repeated indices are summed over. In general, the currents are a function of the intensive parameters (T and τ) as well as the affinities[25] ($\nabla\frac{1}{T}$ and $\nabla\tau$). Thus the heat current $\vec{J}^{(Q)}$ can be expanded in its most general form:

$$J_i^{(Q)} = L_{i,j}^{(Q)} \partial_j \frac{1}{T} + \frac{L_{i,j}^{(\eta_\alpha)}}{T} \partial_j \tau_\alpha + L_{i,j,k}^{(QQ)} \partial_j \frac{1}{T} \partial_k \frac{1}{T}$$
$$+ \frac{L_{i,j,k}^{(Q\eta_\alpha)}}{T} \partial_j \frac{1}{T} \partial_k \tau_\alpha + \frac{L_{i,j,k}^{(\eta_\alpha\eta_\beta)}}{T^2} \partial_j \tau_\alpha \partial_k \tau_\beta. \quad (2)$$

In solids, barring plastic deformation, there is no heat current in steady state solely due to $\nabla\tau_i$. Thus the coefficients $L^{(\eta_\alpha)} = L^{(\eta_\alpha\eta_\beta)} = 0$. Moreover, in symmetric systems, there is no thermal rectification, which implies $L^{(QQ)} = 0$. If we further assume only gradients in the x direction and stress in the y direction, the above equation can be reduced to

$$J_x^{(Q)} = L_{x,x}^{(Q)}\partial_x \frac{1}{T} + \frac{L_{x,x,x}^{(Q\eta_{yy})}}{T} \partial_x \frac{1}{T} \partial_x \tau_{yy}, \quad (3)$$

which leads to different thermal currents when switching the sign of the stress gradient ($\nabla\tau$). For the case of $F_y = 4.8$ nN, the calculated kinetic coefficients are $L_{x,x}^{(Q)} = 1.7 \times 10^8$ WK/m and $L_{x,x,x}^{(Q\eta_{yy})} = 0.34$ WK^2/GPa.

The distinctive property of this approach is the tunability of the thermal rectification by an asymmetrically applied force, F_y. We show in Fig. 6 the thermal rectification factor (TR) as a function of F_y calculated at $T = 300$ K. The TR is defined as

$$\text{TR} = 2\frac{(J_{L\to R} - J_{R\to L})}{(J_{L\to R} + J_{R\to L})} \times 100\%. \quad (4)$$

We observe an increment of the TR when increasing the F_y. The increment of TR with F_y is more prominent at higher biases ($\alpha = 0.3$). As shown in Fig. 5(b), the $J_{L\to R}$ increases almost linearly with the bias (α), whereas $J_{R\to L}$ increases nonlinearly giving rise to a larger TR. This behavior suggests the contribution of higher order terms (beyond the second order) to Eq. (2). The nonlinear transport is an essential property in realizing thermal rectification as in an electronic diode. In our system, the nonlinear transport is prominent at larger F_y's (>0.8 nN), where we observe a clear bias dependence of TR. The maximum TR we observed is about 73%, which occurred at $\alpha = 0.3$ and $F_y = 5.6$ nN.
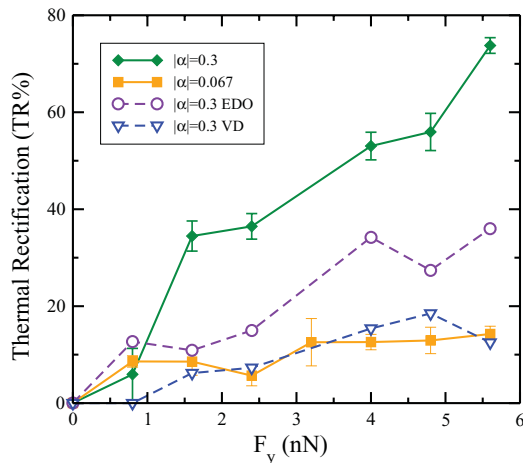
FIG. 6. (Color online) Thermal rectification factor (TR) at $T = 300$ K as a function of F_y. The open circles are in the presence of edge disorder (EDO) and the open triangles are in the presence of vacancy defects (VD).

The right side of the AGNR is subjected to a biaxial stress whereas the left side only has an uniaxial stress. It is evident that the asymmetry of the on axis stresses (σ_R^x and σ_L^x) is important in determining the TR. We achieve a significant TR whenever the ratio $\sigma_R^x/\sigma_L^x \gtrsim 2.0$ [see Fig. 4(b)]. When we move the laterally stressed window towards the center, the TR reduced considerably in our simulation. This is a reasonable observation, because the asymmetry of the system is reduced. For instance, when we move the laterally stressed window eight columns towards the center (keeping the number of atoms that F_y is applied constant) the TR decrease to 5% at $\alpha = 0.3$ and $F_y = 4.8$ nN. In this situation, the ratio of stresses reduces to 1.5 which is close to the ratio at $F_y = 0.8$ nN, where the observed TR is about 6%. When the length of the nanoribbon is increased, the strain gradient reduces and results a reduction of thermal rectification [implies from the Eq. (3)]. However, by increasing the length of the AGNR and also the number of atoms that F_y is applied, we could increase the strain gradient and observe a larger TR.

Graphene commonly possesses edge disorder which significantly degrade the thermal properties. In Fig. 6, the open circles shows the variation of TR in the presence of edge disorder. Since the simulated AGNRs are very small, we introduce only about a 4% (percentage of number of edge atoms removed) edge disorder. We observe moderate reduction of TR, down to a value ~30%. The effect of edge disorder can be reduced by increasing the width of the nanoribbon. However, the presence of vacancy defects significantly reduces the TR. The open triangles in Fig. 6 is for 0.6% vacancy defects distributed evenly in the nanoribbon.

Experimentally, the lateral force on the right half of the AGNR can be applied by coupling to a substrate. Our

simulation fixed the atoms to which the forces were applied. This situation also produces larger thermal rectification (over 100%) at higher biases and the direction of the maximum thermal current is same as before. This effect can be understood by the argument in Ref. 23. Consequently, the observable net thermal rectification could be even higher due to the asymmetric coupling between the GNR and the substrate.

Electronic transport of heat will occur in parallel to the phonon conduction, but is not so large that it dwarfs the phonon channel considered here. In addition, AGNRs shows semiconducting characteristics and their energy gap can be tuned with the strain.[14] Thus the electronic contribution to the thermal transport should not be crucial. Electron-phonon interactions could lead to processes that undermine the thermal rectification. We believe that their contribution to the thermal rectification is also minimal since the nanoribbon is semiconducting. In addition, the long electronic coherence length in graphene indicates that electron-phonon interactions should not be significant. In experiments, these effects can be further minimized by electronically gating the sample.

Finally, we discuss the stability of the C-C bonds in graphene under the lateral forces. We do not observe any rupture of bonds within the applied range of F_y (0–5.6 nN). In our simulation the estimated maximum force in the C-C bond direction is about 6.4 nN, which corresponds to a lateral stress of $\sigma_R^y = 90$ GPa. In a recent experiment, it has been found that the intrinsic strength of a single-layer graphene is about 130 GPa assuming the van der Waals thickness of graphene.[10] When the F_y is increased to 7.2 nN, we observe rupturing of some bonds near the fixed atoms in the right side of the AGNR. At this point, the maximum force in the C-C bond direction is about 8.0 nN. Thus the forces required to realize thermal rectification by our method, are realistic and in an experimentally feasible range.

V. CONCLUSION

In conclusion, we study the thermal transport properties of strained GNRs using MD simulations. We demonstrate that the thermal rectification can be realized by engineering the stress on a rectangular AGNR. We have found that the heat transport is favorable from the less stressed region to the more stressed region. We also found that edge defects and vacancies only partially suppress this rectification. The major advantage of this approach is that the thermal rectification can be tuned from no rectification state to over 70% in real-time by applying a mechanical force.

*harsha@ou.edu

[1]M. Terraneo, M. Peyrard, and G. Casati, Phys. Rev. Lett. **88**, 094302 (2002).

[2]B. Li, L. Wang, and G. Casati, Appl. Phys. Lett. **88**, 143501 (2006).

[3]L. Wang and B. Li, Phys. Rev. Lett. **101**, 267203 (2008).

[4]L. Wang, and B. Li, Phys. World **21**, 27 (2008).

[5]J. Hu, X. Ruan and Y. P. Chen, Nano Lett. **9**, 2730 (2009).

[6]N. Yang, G. Zhang, and B. Li, Appl. Phys. Lett. **95**, 033107 (2009).

[7]C. W. Chang, D. Okawa, A. Majumdar, and A. Zettl, Science **314**, 1121 (2006).

[8]A. K. Geim and K. S. Novoselov, Nat. Mater. **6**, 183 (2007).

[9]A. A. Balandin *et al.*, Nano Lett. **8**, 902 (2008).

[10]C. Lee, X. Wei, J. W. Kysar, and J. Hone, Science **321**, 385 (2008).

[11]F. Guinea, A. K. Geim, M. I. Katsnelson, and K. S. Novoselov, Phys. Rev. B **81**, 035408 (2010).

[12]T. Low and F. Guinea, Nano Lett. **10**, 3551 (2010).

[13]N. Levy, S. A. Burke, K. L. Meaker, M. Panlasigui, A. Zettl, F. Guinea, A. H. Castro Neto, and M. F. Crommie, Science **329**, 544 (2010).

[14]G. Gui, J. Li, and J. Zhong, Phys. Rev. B **78**, 075435 (2008).

[15]Z. Guo, D. Zhang, and X-G. Gong, Appl. Phys. Lett. **95**, 163103 (2009); X. Li, K. Maute, M. L. Dunn, and R. Yang, Phys. Rev. B **81**, 245318 (2010); N. Wei, L. Xu, H-Q. Wang, and J-C. Zheng, Nanotechnology **22**, 105705 (2011).

[16]R. Gillen, M. Mohr, J. Maultzsch, and C. Thomsen, Phys. Status Solidi B **246**, 2577 (2009).

[17]D. W. Brenner, Phys. Rev. B **42**, 9458 (1990).

[18]G. Wu and B. Li, Phys. Rev. B **76**, 085424 (2007).

[19]W. Bao, F. Miao, Z. Chen, H. Zhang, W. Jang, C. Dames, and C. N. Lau, Nat. Nanotechnology **4**, 562 (2009).

[20]C. C. Chen, W. Bao, J. Theiss, C. Dames, C. N. Lau, and S. B. Cronin, Nano Lett. **9**, 4172 (2009).

[21]T. M. G. Mohiuddin, A. Lombardo, R. R. Nair, A. Bonetti, G. Savini, R. Jalil, N. Bonini, D. M. Basko, C. Galiotis, N. Marzari, K. S. Novoselov, A. K. Geim, and A. C. Ferrari, Phys. Rev. B **79**, 205433 (2009); M. Huang, H. Yan, C. Chen, D. Song, T. F. Heinz, and J. Hone, Proc. Natl. Acad. Sci. USA **106**, 7304 (2009).

[22]R. C. Picu, T. Borca-Tasciuc, and M. C. Pavel, J. Appl. Phys. **93**, 3535 (2003).

[23]D. B. Go and M. Sen, J. Heat Transfer **132**, 124502 (2010).

[24]D. Wallace, *Thermodynamics of Crystals* (Wiley, 1972), p. 17.

[25]H. B. Callen, *Thermodynamics and an Iintroduction to Thermostatistics*, 2nd ed. (Wiley, 1985), p. 307.